An insight into the common mechanism of the chromophore formation in the red fluorescent proteins: The elusive blue intermediate revealed. Supporting Information.

Ksenia B. Bravaya, Oksana M. Subach, Nadezhda Korovina, Vladislav V. Verkhusha, and Anna I. Krylov

January 8, 2012

1 List of supporting tables and figures

2 Supporting results and discussion

2.1 Ground state equilibrium geometries and the effect of methylation

The values of the relevant structural parameters including bond lengths in the π-system and important dihedral angles (Fig. S2) for model chromophores are summarized in Tables S1 and S2.

Methylation causes steric repulsion between the methyl group and the carbonyl moiety leading to deviation from planarity at the acylimine fragment. The dihedral angles describing the degree of non-planarity of the optimized structures of model chromophores are given in Tables S1 and S2. Interestingly, the HIMA oxidized cation in strongly non-planar even in the non-methylated state (HIMAo). The degree of non-planarity depends on the protonation state.

The concept of resonance (mesomeric) interactions can be used to rationalize the equilibrium structures as well as ground- and excited-state properties of conjugated molecules. The electronic structure of the anionic and zwitterionic chromophores can be described by two resonance forms: in one, the negative charge is located on imidazolinone ring, and in the other — on the enol-group of the acylimine fragment (Fig. S2). This affects bond length alternation (BLA) in the acylimine region leading to shortening of the single bonds and elongating the double bonds relative to the bonds of pure single and double character. The neutral and doubly-oxidized structures [(m)HIMAn and (m)HIMAo] are dominated by a single resonance form, and one can expect larger BLA at the acylimine fragment. The cationic structures (mHIMAc and HIMAc) have two resonance forms, however, the acylimine moiety is not involved, and one can expect that BLA in the cationic, neutral and doubly-oxidized chromophores will be similar.

To quantify the degree of BLA at the acylimine moiety, we define the BLA^{AI} parameter as a difference between the sum of the two formal single and two formal double bond lengths [b+d-(a+c), Fig. S1] according to structural representation in Fig. S1. In line with the resonance structures analysis, BLA^{IA} is much smaller for the anionic and zwitterionic forms than for the cationic, neutral and doubly-ionized chromophores (Tables S1 and S2). BLA^{AI} reaches its smallest value for HIMAzwA (0.150) and mHIMAzwA (0.146) where the negative charge on the enol moiety is stabilized by the positive charge of the protonated nitrogen. Note that bond c is 0.047-0.099 and 0.038-0.089 Å longer in mHIMAzwA and HIMAzwA, respectively, than in other protonation/oxidation states of the chromophore illustrating the trend to the reverse BLA (relative to the BLA pattern shown in Fig. S1) in this zwitterionic form. This is also reflected by the values of the equilibrium dihedral θ and φ angles. For all the mHIMA structures, except mHIMAzwA, the chromophore is twisted along the θ angle, whereas φ is close to 180° (Tables S1 and S2). In contrast, θ is only 6° in mHIMAzwA, whereas φ reaches 155°. Thus, C1–N bond is more flexible in mHIMAzwA.

As the methylation results in non-planarity of the chromophore involving its π-conjugated system, one can expect significant effects on the vertical excitation energies, which is discussed below.

2.2 Vertical excitation energies

The lowest bright excited state of the HIMA chromophores corresponds to the $\pi\pi^*$ transition involving molecular orbitals that are similar in all protonation states, except doubly-oxidized chromophore, (m)HIMAo, which has two less electrons in the π-system. Consequently, its highest occupied π-orbital is one of the occupied π-orbitals lying below HOMO in other systems and its lowest vacant π^* orbital is similar to the highest occupied π orbital of other HIMA chromophores (Fig. S3).

In most of the chromophores, the π-π^* excitation gives rise to the lowest singlet excited state. The only exceptions are the cations, which feature a number of dark n-π^* excited states lying below the bright excited state, as illustrated in Fig. S4. This is caused by stabilization of the of π-orbitals on the imidazolinone ring by the positive charge delocalized over the π-system, whereas the lone pair orbital energies are shifted less.

Vertical excitation energies computed for the methylated and non-methylated forms of the chromophores are given in Table S3. The lowest bright excited states of both anionic chromophores (HIMAa and mHIMAa) lie above the corresponding vertical detachment energies (2.88 and 2.74 eV at the ωB97X-D/aug-cc-pVDZ level, respectively). This requires special treatment of these resonance (i.e., unstable with respect to electron detachment) excited states. For example, using diffuse bases leads to strong mixing between the valence excited states and artificial states representing the detachment continuum.[1,2] This affects both the excitation energies and oscillator strengths. More reliable estimates can be obtained by using the basis sets without diffuse functions (the cc-pVDZ and cc-pVTZ bases was used for the description of (m)HIMAa excited states). This is equivalent to stabilization of the valence excited states with respect to the continuum.

Extension of the basis set from 6-31+G(d) to aug-cc-pVTZ results in small changes in excitation energies (within 0.2 eV) for all model systems. Moreover, the aug-cc-pVTZ and aug-cc-pVDZ excitation energies lie within 0.1 eV with systematic decrease in excitation energy upon transition to a larger aug-cc-pVTZ basis. The SOS-CIS(D) results were validated by the comparison with EOM-EE-CCSD excitation energies. Due to the N^6 scaling, the EOM-CCSD calculations are more demanding and a small 6-31+G(d) basis was used. As follows from Table S3, the EOM-EE-CCSD excitation energies are systematically higher (by 0.02–0.22 eV) than the corresponding SOS-CIS(D) values, due to a known trend of EOM-CCSD to overestimate excitation energies of the valence excited states. The oscillator strength and the leading wave function amplitudes are in qualitative agreement between the two methods, which demonstrates that the CIS wave functions are qualitatively correct and, therefore, the SOS-CIS(D) results are reliable. Thus, the assignment of the experimental bands using the SOS-CIS(D) energies is justified.

The comparison of the computed SOS-CIS(D)/aug-cc-pVDZ (cc-pVDZ for anions) vertical excitation energies for both methylated and non-methylated model systems and experimental absorption spectrum of the DsRed blue form reveals that only anionic and zwitterionic (zwI) forms can be responsible for the absorption of the blue form.

2.3 The effect of non-planarity on excitation energies

As the chromophore non-planarity disturbs the conjugated π-system, it is important to analyze the effect of geometry distortion on the excitation energies of the chromophore. Moreover, chromophore's thermal motions, such as flexible out-of-plane vibrations disrupting the planar conjugated π-system, can result in the broadening of the spectrum. Thus, we analyzed the effect of non-planarity on the ground and excited electronic states for the anionic and neutral forms of (m)HIMA chromophores. The RIMP2/cc-pVTZ optimized geometries were used in calculations of the rotation energy profiles. The profiles were computed with long-range corrected DFT (ωB97X-D/aug-cc-pVDZ, Ref. 3) by varying the C12–N13–C14–O15 dihedral angle (θ, see Fig. S1) with all other degrees of freedom being frozen.

The energy profiles for the ground electronic states computed for θ varying from 0 to 106° as well excitation energies at critical θ (0°, equilibrium value, 106°) are shown in Fig. S6. The observed ground-state behavior of the chromophore in different protonation/oxidation states with respect to rotation along the θ angle is consistent with the BLA pattern discussed above. mHIMAa and mHIMAzwA are nearly planar in the ground state which is in agreement with the lowest BLA^{AI}(Table S2) for these two forms (0.192 and 0.146 Å, respectively). Relative energy of the planar geometry w.r.t. the equilibrium one increases in the series mHIMAzwI<mHIMAn<mHIMAc<mHIMAo following the trend of the BLA^{AI} increase. Upon the BLA^{AI} increase bond c becomes longer making the chromophore more flexible. This results in a less planar equilibrium structure and, taking into account steric repulsion between methyl group and acylimine carbonyl, causes higher energy of the planar structure relative to the equilibrium geometry.

The mHIMAa excitation energies depend only slightly on the θ values (2.95–3.13 eV), whereas the effect of the chromophore non-planarity on excitation energies of mHIMAn (3.85–4.48 eV) is much stronger. This can be explained by the analysis of the CIS attachment/detachment densities (Figs. S7,S8). For the anionic chromophore the main electron density redistribution occurs at the imidazolinone ring and the C2–N bond for all three geometries (planar, equilibrium and twisted corresponding to the protein value of dihedral angle), and, therefore, this transition is not affected by rotation along the acylimine N–C3 bond. For the neutral chromophore at planar geometry, the electron density redistribution upon excitation involves acylimine fragment, whereas it becomes more localized as the acylimine moiety is twisted along N–C3 leading to the excitation energy increase. The excitation energy shifts for other protonation/oxidation states caused by rotation along θ vary from 0.1 to 0.5 eV. We observe similar magnitude effects in the non-methylated species (Fig. S6).

2.4 The role of K70(R70) residues in stabilization of the anionic intermediate

Fig. S9 shows the active site of mTagBFP, which is considered to be similar to the blue intermediate[4,5] in the RFPs maturation process. Chromophore's enol oxygen negative charge is stabilized by interactions with Arg95 and Lys70. Moreover, positively charged residue is found at this position in a number of red FPs. Alignment of the amino acid sequences of red FPs with GFP, Fast-FT and mTagBFP is shown in Fig. S10. Alignment numbering follows that of DsRed. Residues buried in β-can are shaded. Stars indicate residues forming the chromophore. β-sheet forming regions and α-helixes are denoted as arrows and ribbons, respectively. Amino acids that can participate in stabilization of the blue form are highlighted by cyan color.

2.5 Chromophore stability inside the mTagBFP protein matrix: different protonation states

To assess the chromophore stability inside the protein matrix, geometry optimizations of mTagBFP with the chromophore in anionic (mHIMAa), zwitterionic (mHIMAzwI) and 2-electron oxidized states (mHIMAo) were performed. The optimized geometry of mTagBFP with the anionic chromophore is in good agreement with the X-ray structure. However, both zwitterion and doubly-oxidized cation were found to be unstable. Resulting structures for zwitterion and doubly-oxidized cation are shown in Fig S11. Zwitterionic structure undergoes proton transfer to Glu215, whereas 2-electron oxidized cation is destroyed by the nucleophilic addition of the OH group from the nearby water molecule (the shown structure of doubly-oxidized cation is not a stationary point: the gradient value is 0.0089).

Supporting tables and figures

Table S1: Relevant structural parameters for the RI-MP2/cc-pVTZ optimized geometries of non-methylated HIMA: θ, φ (degrees); a–j, BLA (Å). See Fig. S1 for definition of the geometric parameters.

	HIMAn	HIMAa	HIMAc	HIMAzwI	HIMAzwA	HIMAo
φ	175	180	178	180	180	177
θ	35	0	30	0	0	50
a	1.216	1.236	1.209	1.216	1.212	1.205
b	1.422	1.378	1.460	1.417	1.384	1.462
c	1.295	1.333	1.284	1.301	1.371	1.282
d	1.424	1.386	1.437	1.391	1.349	1.459
e	1.378	1.384	1.356	1.355	1.382	1.302
f	1.356	1.393	1.363	1.414	1.382	1.475
g	1.353	1.245	1.331	1.224	1.221	1.190
h	1.392	1.449	1.389	1.433	1.474	1.521
i	1.354	1.333	1.364	1.346	1.303	1.292
j	1.345	1.368	1.351	1.363	1.384	1.417
BLA^{AI} [a]	0.335	0.195	0.404	0.291	0.150	0.434

[a] Bond length alternation in the acylimine region = $b + d - a - c$

Table S2: Relevant structural parameters for the RI-MP2/cc-pVTZ optimized geometries of methylated mHIMA: θ, φ (degrees); a–j, BLA (Å). See Fig. S1 for definition of the geometric parameters.

	mHIMAn	mHIMAa	mHIMAc	mHIMAzwI	mHIMAzwA	mHIMAo
φ	176	170	174	171	155	174
θ	67	20	60	42	6	75
a	1.217	1.238	1.211	1.220	1.213	1.207
b	1.404	1.366	1.431	1.390	1.380	1.441
c	1.293	1.337	1.285	1.302	1.384	1.287
d	1.444	1.401	1.457	1.407	1.363	1.472
e	1.397	1.386	1.357	1.360	1.390	1.304
f	1.359	1.396	1.366	1.414	1.384	1.472
g	1.356	1.246	1.332	1.225	1.222	1.191
h	1.387	1.445	1.385	1.430	1.467	1.519
i	1.358	1.335	1.366	1.346	1.304	1.291
j	1.342	1.367	1.350	1.364	1.381	1.420
BLA^{AI} [a]	0.338	0.192	0.392	0.275	0.146	0.419

[a] Bond length alternation in the acylimine region $= b + d - a - c$

Table S3: Vertical excitation energies for the HIMA and mHIMA chromophores computed at different levels of theory.

Molecule	SOS-CIS(D)/						EOM-CCSD/	
	aug-cc-pVTZ		aug-cc-pVDZ		6-31+G(d)		6-31+G(d)	
	E, eV (nm)	f_L	E, eV	f_L	E, eV	f_L	E, eV	f_L
HIMAn	3.93 (316)	0.82	4.00	0.82	4.09	0.82	4.30	0.54
HIMAa	2.97 (418)	1.25	3.00	1.14	3.01	1.25	3.35	1.02
HIMAc	4.24 (293)	0.80	4.34	0.80	4.45	0.83	4.61	–
HIMAzwI	2.92 (425)	1.03	2.98	1.03	3.03	1.09	3.25	0.80
HIMAzwA	4.01 (310)	1.19	4.07	1.20	4.18	1.25	4.32	0.82
HIMAo	5.51 (225)	0.87	5.59	0.87	5.62	0.88	5.63	0.49
mHIMAn	4.37 (284)	0.64	4.43	0.62	4.50	0.70	–	–
mHIMAa	2.85 (436)	1.14	2.95	1.20	2.89	1.15	–	–
mHIMAc	4.44 (280)	0.71	4.54	0.71	4.65	0.74	–	–
mHIMAzwI	2.93 (424)	0.90	3.00	0.90	3.06	0.97	–	–
mHIMAzwA	3.88 (320)	1.19	3.94	1.19	4.03	1.26	–	–
mHIMAo	5.13 (242)	0.65	5.19	0.65	5.22	0.67	–	–

cc-pVDZ and cc-pVTZ bases were used for anions.
Equilibrium geometries: RI-MP2/cc-pVTZ.

Table S4: Excitation energies, eV, and oscillator strengths (in parentheses) for the isolated (QM) and protein-bound (QM/MM) anionic chromophore. The aug-cc-pVDZ basis set was used in all calculations.

QM		QM/MM	
CIS	SOS-CIS(D)	CIS	SOS-CIS(D)
4.18 (0.61)	3.08	4.28 (0.76)	3.11

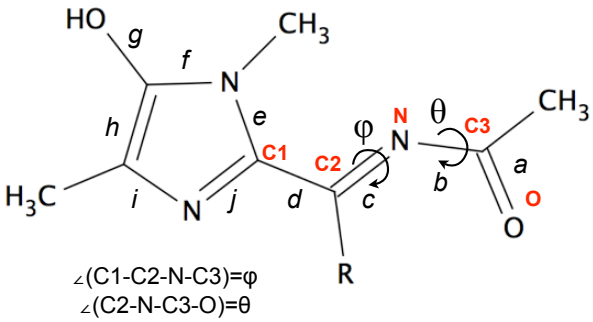

Figure S1: Definition of relevant structural parameters.

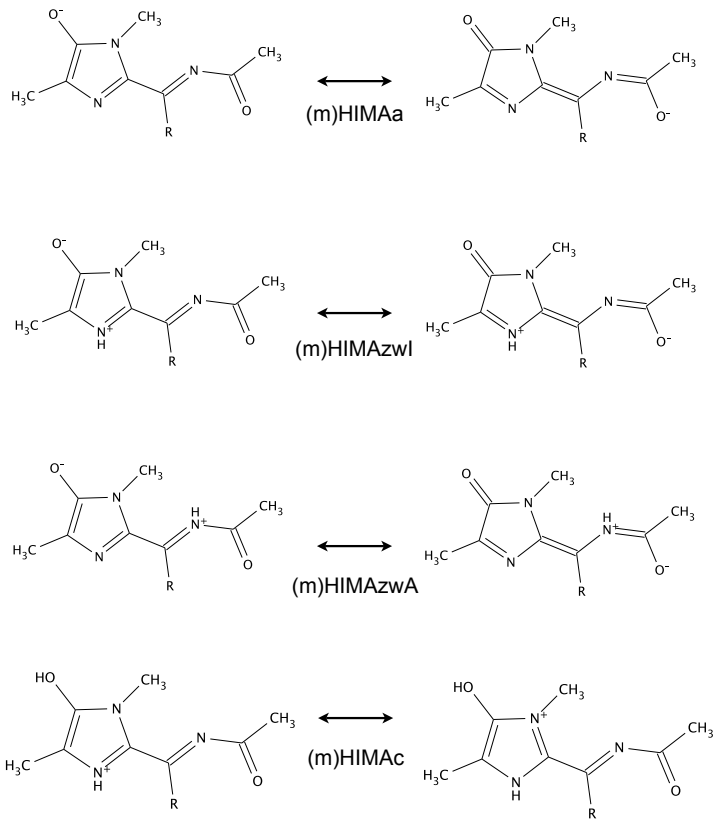

Figure S2: Relevant resonance structures for the anionic (m)HIMAa chromophore. The anionic and zwitterionic forms of the HIMA chromophore can be represented by two similar resonance forms (HIMAa, HIMAzwI, HIMAzwA, mHIMAa, mHIMAzwI and mHIMAzwA).

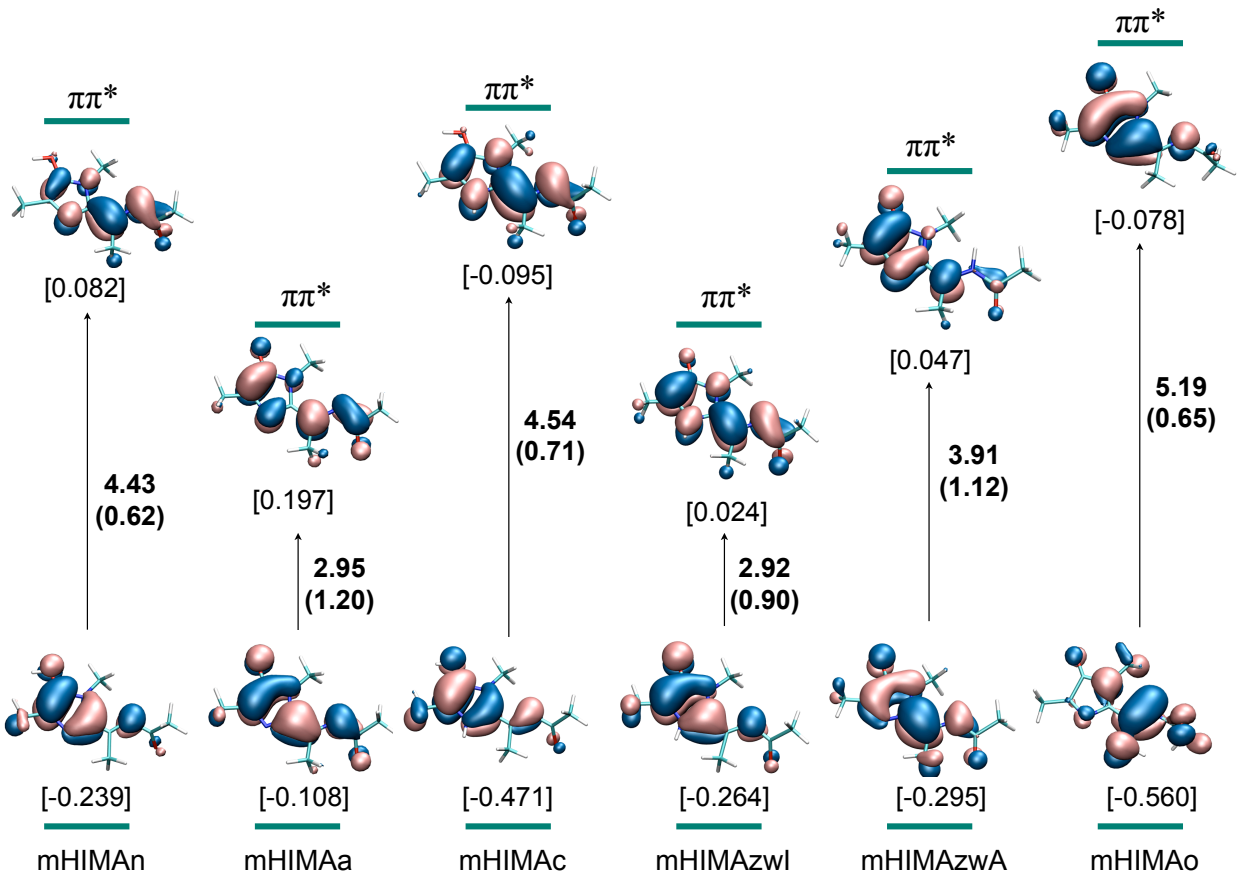

Figure S3: The HF/aug-cc-pVDZ molecular orbitals involved in the bright π-π^* transitions for mHIMA in different protonation and oxidation states. Shown are SOS-CIS(D)/aug-cc-pVDZ excitation energies (eV). CIS/aug-cc-pVDZ oscillator strengths are given in parentheses. Orbital energies (hartree) are shown in square brackets.

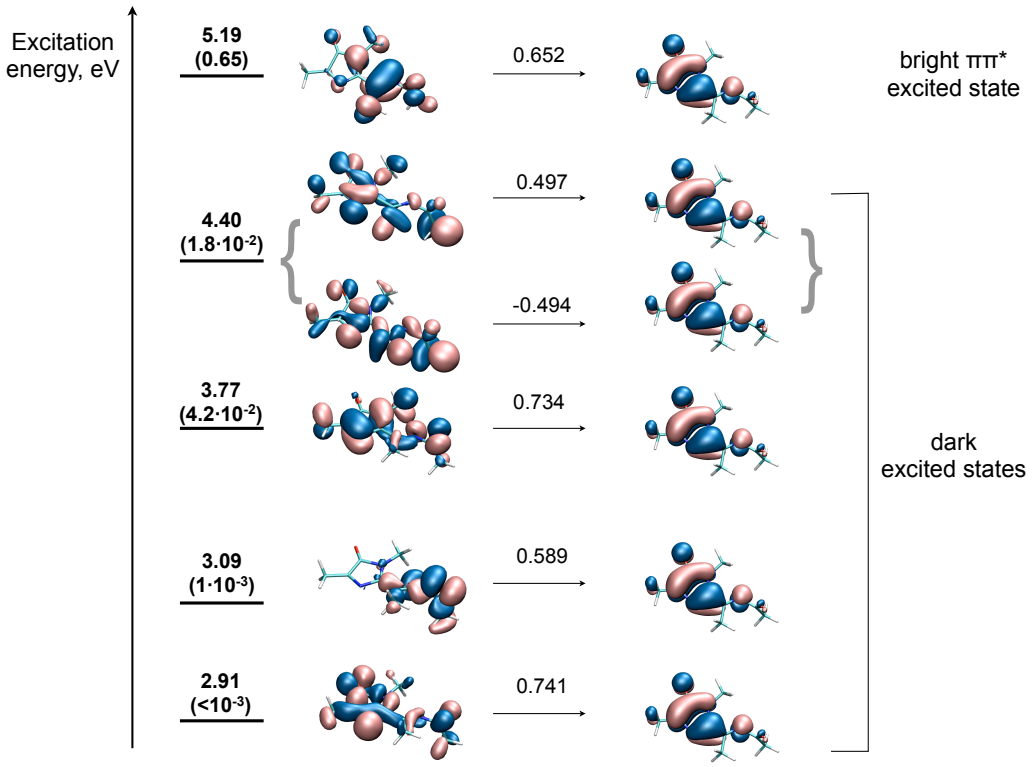

Figure S4: The SOS-CIS(D)/aug-cc-pVDZ excitation energies (eV) for different dark mHIMAc excited states states lying below the bright $\pi\pi^*$ state. CIS/aug-cc-pVDZ oscillator strengths are given in parentheses. The CIS/aug-cc-pVDZ amplitudes are shown above arrows.

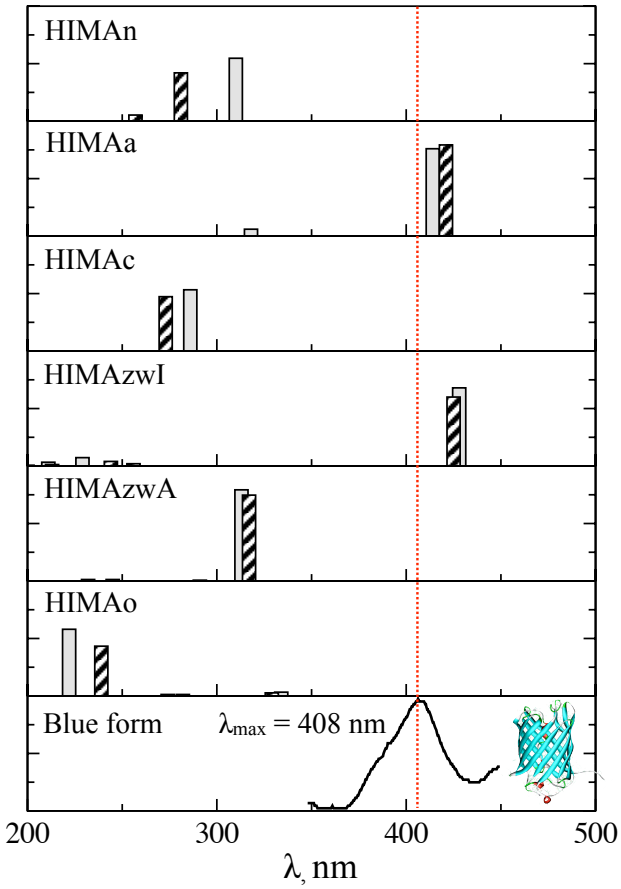

Figure S5: The SOS-CIS(D)/aug-cc-pVDZ excitation energies for HIMA, R=H (solid), R=CH_3 (dashed), in different protonation and oxidation states. The bar heights are proportional to oscillator strengths. The experimental spectrum for the blue form of DsRed (bottom panel) is from Ref. 6.

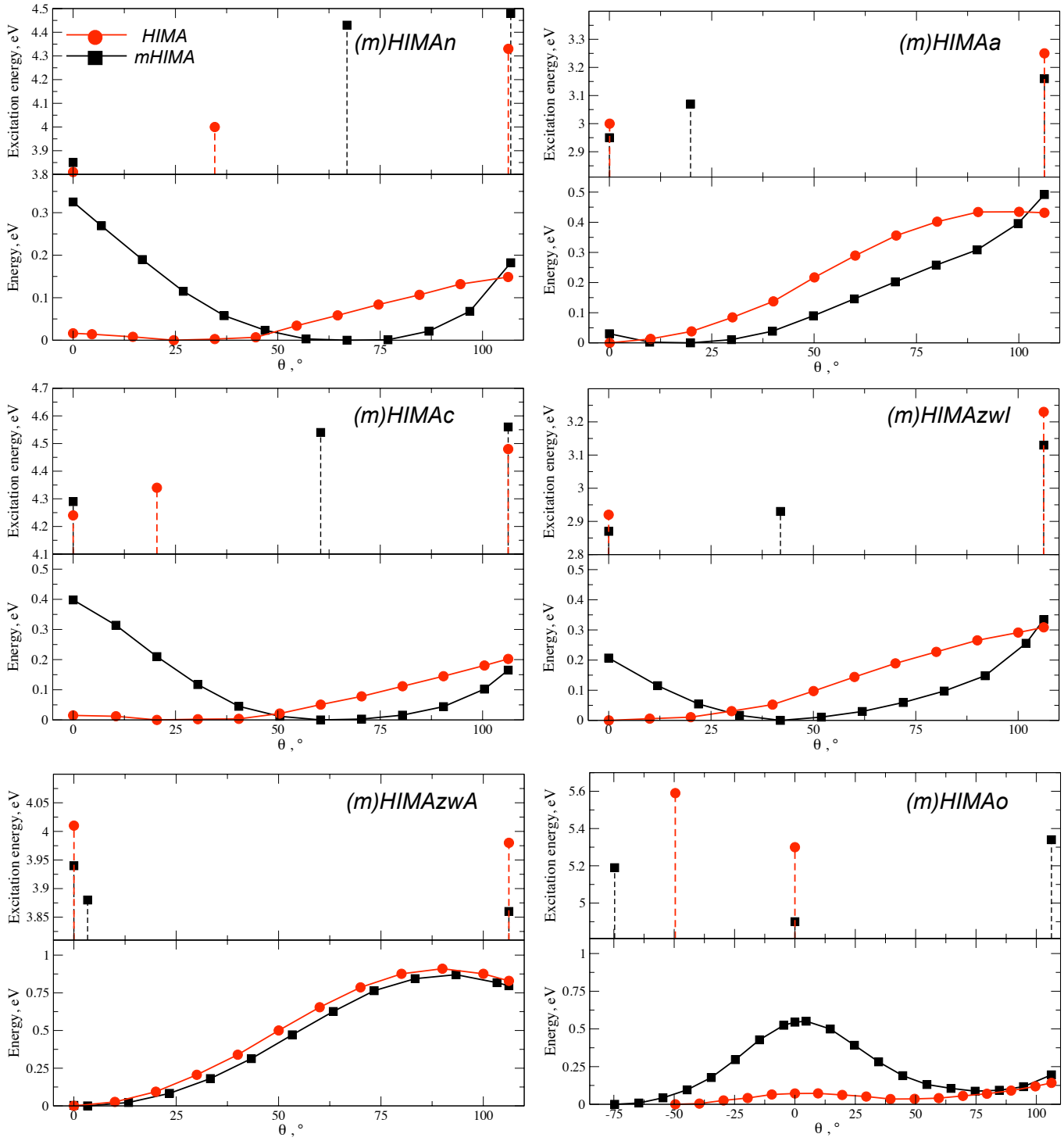

Figure S6: The ground state (bottom) and excitation energies (top) for different θ values.

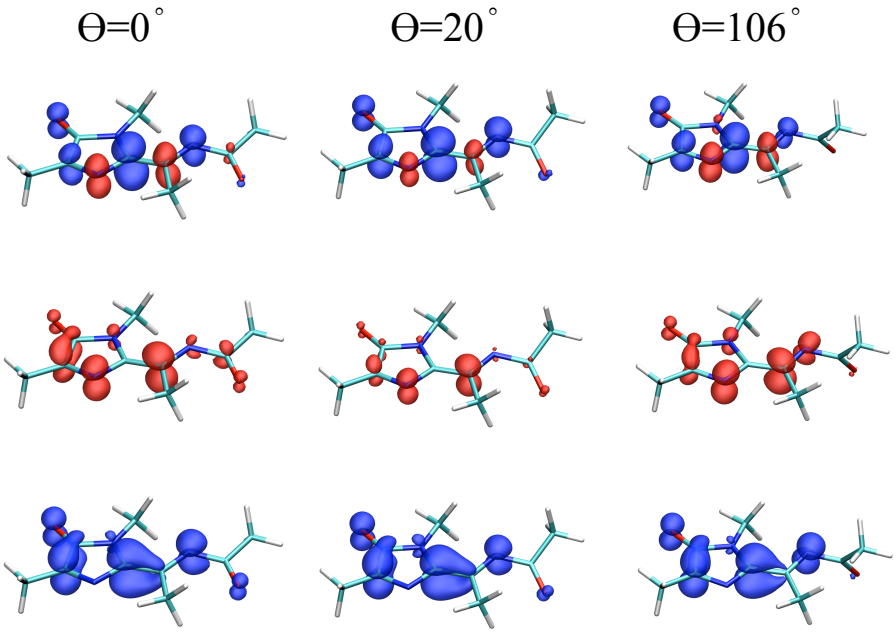

Figure S7: The CIS/aug-cc-pVDZ detachment (describing electron removal from the ground electronic state, bottom), attachment (corresponding to charge rearrangement in the excited electronic state, middle) and differential density (top) for the planar, equilibrium and twisted structures of mHIMAa.

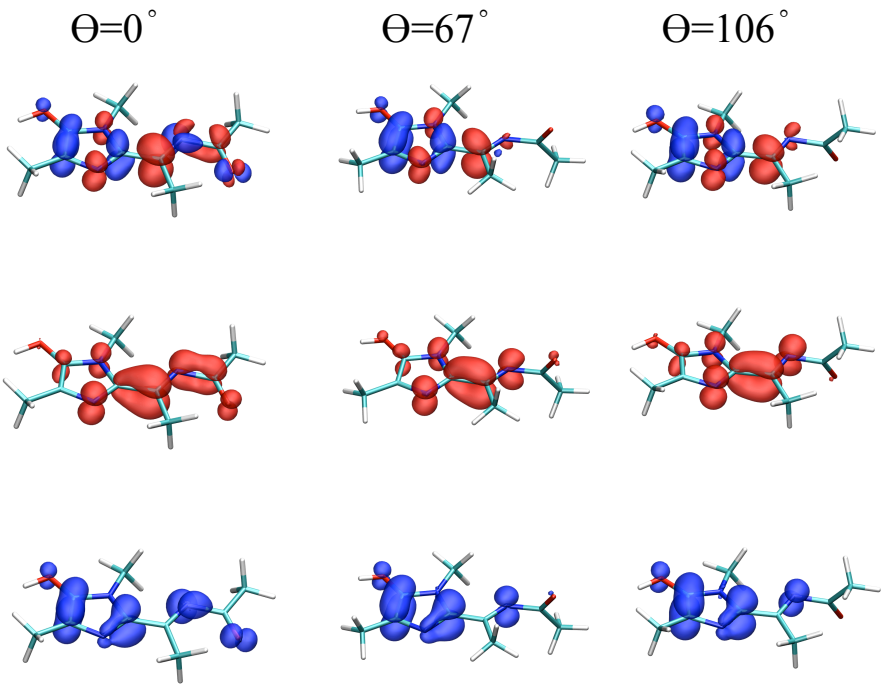

Figure S8: The CIS/aug-cc-pVDZ detachment (describing electron removal from the ground electronic state, bottom), attachment (corresponding to charge rearrangement in the excited electronic state, middle) and differential density (top) for planar, equilibrium and twisted structures of mHIMAn.

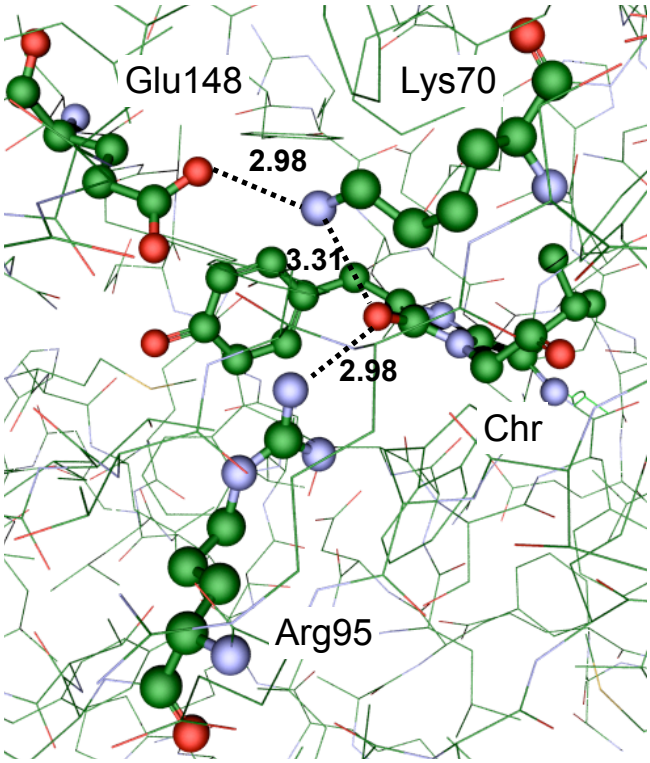

Figure S9: Active site of mTagBFP (3M24 PDB ID, Unit A), Ref. 5.

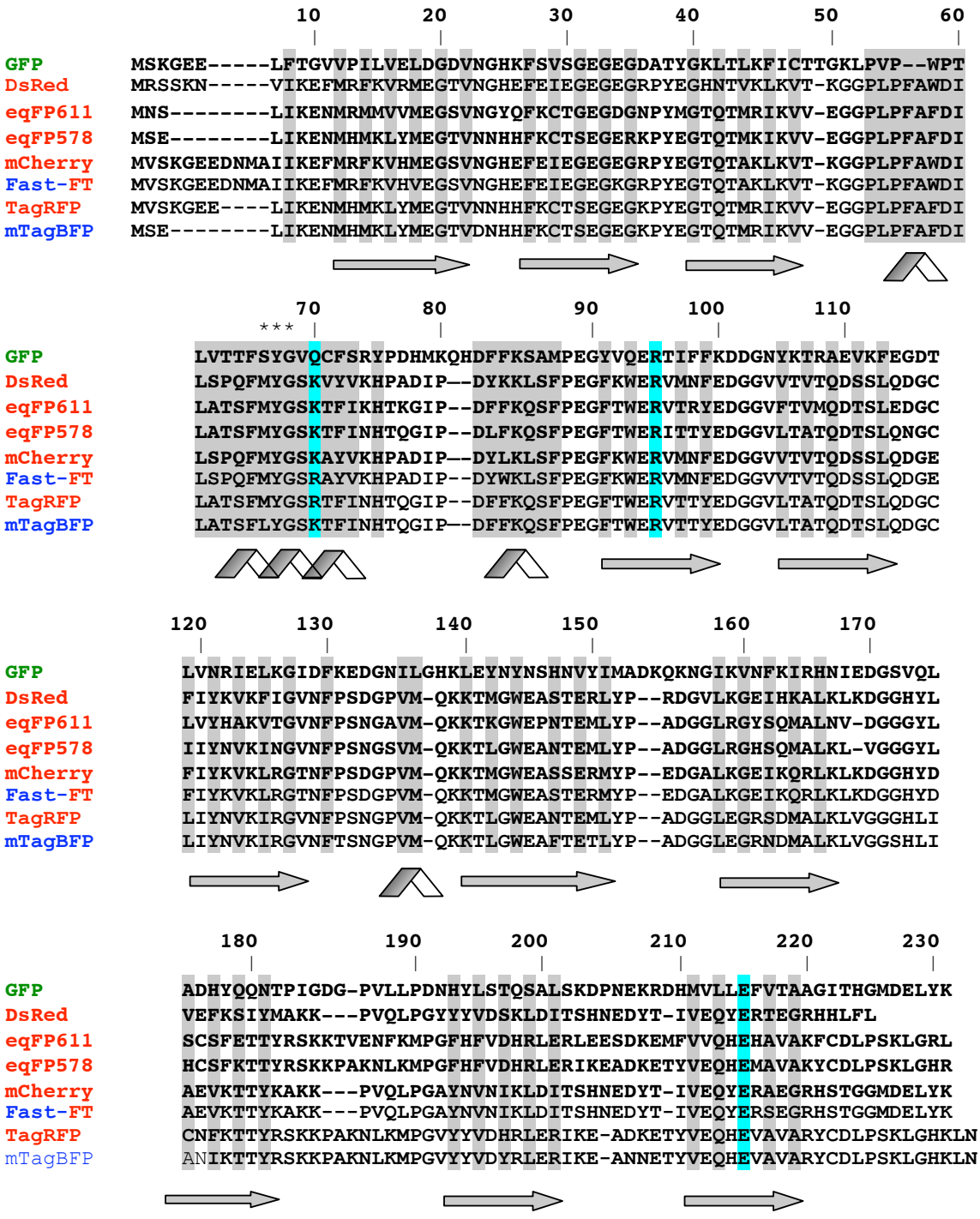

Figure S10: Alignment of the amino acid sequences of red FPs with GFP, Fast-FT and mTagBFP.

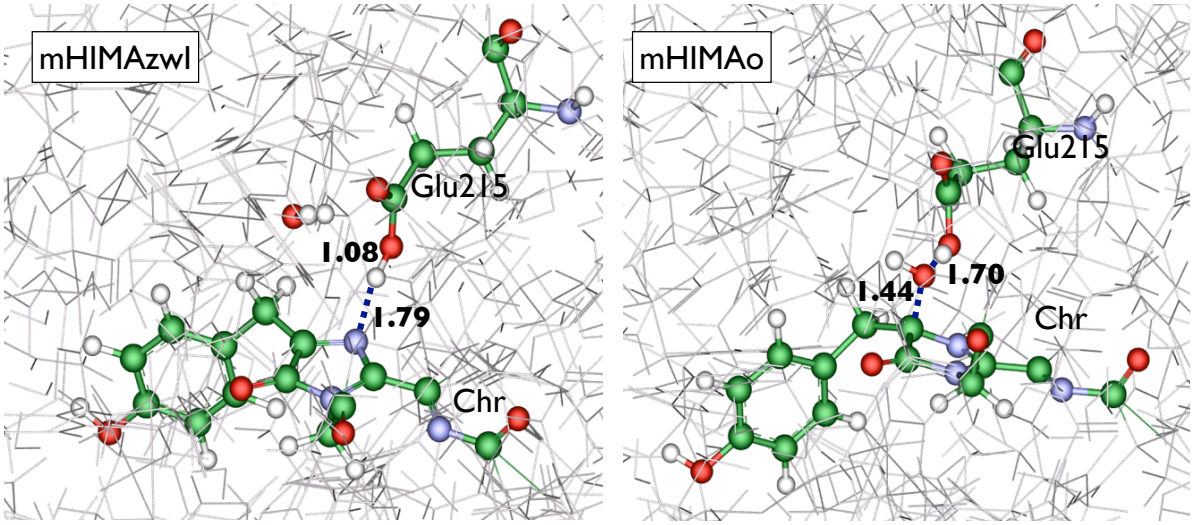

Figure S11: mTagBFP structures resulting from mTagBFP geometry optimization with the chromophore in zwitterionic (left) and doubly-oxidized (right) states.

References

[1] Epifanovsky, E. ; Polyakov, I. ; Grigorenko, B.L. ; Nemukhin, A.V. ; Krylov, A.I. *J. Chem. Theory Comput.* **2009**, *5*, 1895.

[2] Zuev, D. ; Bravaya, K.B. ; Crawford, T.D. ; Lindh, R. ; Krylov, A.I. *J. Chem. Phys.* **2011**, *134*, 034310.

[3] Chai, J.-D. ; Head-Gordon, M. *Phys. Chem. Chem. Phys.* **2008**, *10*, 6615.

[4] Subach, O. M. ; Gundorov, I. S. ; Yoshimura, M. ; Subach, F. V. ; Zhang, J. ; Grüenwald, D. ; Souslova, E. A. ; Chudakov, D. M. ; Verkhusha, V. V. *Chem. Biol.* **2008**, *15*, 1116.

[5] Subach, O. S. ; Malashkevich, V. N. ; Zencheck, W. D. ; Morozova, K. S. ; Piatkevich, K. D. ; Almo, S. C. ; Verkhusha, V. V. *Chem. Biol.* **2010**, *17*, 333.

[6] Verkhusha, V. V. ; Chudakov, D. M. ; Gurskaya, N. G. ; Lukyanov, S. ; Lukyanov, K. A. *Chem. Biol.* **2004**, *11*, 845.